

# In-situ monitoring of internal displacements by FBG sensors and slope stability analysis under rainfall infiltration

Dongsheng Xu, Fei Tong, Huahu Pei, and Jianhua Yin

Department of Civil and Structural Engineering, The Hong Kong Polytechnic University, Hong Kong, China

E-mail: 10900206r@connect.polyu.hk

**ABSTRACT:** The Wenchuan earthquake in Sichuan Province of China has caused tremendous loss of life and property. The severe earthquake along with the heavy rainfall has induced landslide and debris flows so that the slope stability is a significant concern in this earthquake region. A newly developed inclinometer based on the Fiber Bragg Grating (FBG) sensing technique has been installed in a slope in Sichuan Province for long-term monitoring of internal displacements. A series of FBG sensing bars are installed at different depths of two different boreholes in the slope; meanwhile, all optical fibers of the sensing bars are connected and extended to a monitoring station around 1000m away from the slope site through a main armored cable of optical fibers. Monitoring works are carried out in the monitoring station from 20 June to 25 September 2010. Thus, internal displacements of the slope are analyzed together with the rainfall data which are also collected by a rainfall gauge. The results demonstrate that rainfall infiltration has a strong influence on the internal displacements, while the influence reduces dramatically when the depth exceeds 5.2m. Through a numerical model for the effect analysis of rainfall intensity and duration, the slope stability decreases significantly when the rainfall intensity higher (or equal) than 0.5mm/h and rainfall duration longer than 100h.

## 1. INTRODUCTION

Landslide imposes a great threat to the human life and property, thus, numerous researches have been conducted in slope stability analysis. Theoretical studies indicate that slope sidings are caused by various factors including geologic structure, geometry, soil properties, rainfall infiltration, evaporation and earthquake (e.g. Morgenstern, 1965; Sarma, 1973; Greco, 1996; Zheng et al., 2009). Leonardo et al. (2010) reported that the slow-moving was dominated by the pore water pressure and has a close relationship with seasonal variation. Former researchers such as Collins (2004), Tohari (2007), Frattini (2009), and Arezoo (2010) convinced that rainfall and evaporation have indispensable impact on the slope stability. Many finite element methods (FEM) were also used by pervious researchers to study the slope stability (Hovland, 1977; Zhang, 1988; Huang and Tsai, 2000; Chang, 2002).

In addition to the theoretical analysis, geotechnical monitoring provides a direct way to understand the slope behavior. The inclinometer is one of the most common used instruments to measure the slope deformation normal to the axis of borehole casing. Traditional inclinometers are based on the electric servo-accelerometer probe or solid-state micro-electro-mechanical-sensors (MEMS). However, some limitations have been involved by using electric sensors, such as electromagnetic interference and signal loss for long distance transmission. With the development of fiber optic sensing technology, these limitations can be overcome by employing fiber optic sensors. The fiber Bragg grating (FBG) sensor has been widely applied in this area due to the intrinsic merits, such as high sensibility to the strain and temperature, small volume, light weight, resistance to the corrosion and electromagnetic interference (Yin, 2008; Zhu, 2010). In this study, the newly in-place inclinometer is developed with FBG sensors and installed in a typical slope in the Beichuan earthquake area in China for long-term monitoring. Along with the displacement monitoring, the rainfall data of this slope are recorded for analyzing the effect of rainfall infiltration. Additionally, the laboratory tests are conducted to examine the shear strength properties of soil in the slope. Finally, based on slope geometry and soil properties, the numerical simulation model is established to evaluate the influence of rainfall intensity and duration on slope stability.

## 2. SITE DESCRIPTION

In this study, the slope is located in the Weijia gully area with 2 km away from Beichuan city which is a hilly area in the southwest of China. Due to the heavy Wenchuan earthquake on 12th May 2008, the slope become unstable and the geomaterials in the surface layers of the slope become loose (Zhuang et al. 2010; Cui et al. 2011). In this area, the mainly rainy season is from June to September, which

is about 74% of the annual rainfall during this period (Cui et al., 2011). Four month after the earthquake, an extremely heavy rainfall occurred on September 23 and 24 2008 which triggered the debris flow in this Weijia gully. According to the records, the daily rainfall on the September 23 is 173.8mm and the rainfall is 98.9 mm from 0:00 to 6:00 on Sept. 24 (Cui et al. 2011). The Weijia gully was filled with the debris flow on average 3m of the depth. To make matters worse, a part of Beichuan city including the Beichuan High School was burned by this debris flow (Cui et al., 2011).

The main sources of the debris flow are the landslides at the both sides of the Weijia gully. The Weijia gully is flow into the QianJiang from North to South with the 'U' shape of gulches. The drainage conduits had been constructed before the earthquake with the depths of 5~8m and length of 2 km. After the debris flow, all these conduits have been damaged and many loose geomaterial filled with the conduits. According to the investigation report provided by the Sichuan geological engineering survey court, the total volume of this debris flow in Weijia gully is  $10.5 \times 10^4 \text{m}^3$ , in which, the volume of landslide in this studied slope is  $8.5 \times 10^4 \text{m}^3$  (i.e. 80.95% of the total volume) (Zhuang et al. 2010). A geotechnical investigation was carried out after the debris flow. The investigations include drilling two boreholes, studying the soil properties, and installing in-place inclinometers. The longitudinal section of the slope and locations of two investigation boreholes are shown in Figure 1. After the investigations, borehole A and B are installed FBG based in-place inclinometers for long-term monitoring of the slope.

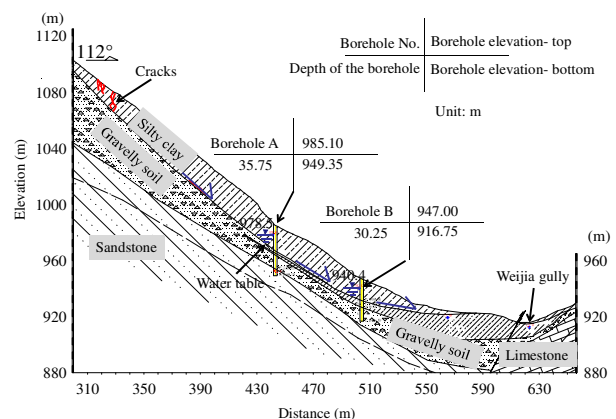


Figure 1 Longitudinal section of the slope and locations of boreholes A and B

3. SOIL PROPERTIES OF THE SLOPE

Samples taken from the drill hole were carried out laboratory tests following the BS 1377:1990. The specific gravity of sand-gravel soil is 2.72, the liquid limit  $w_L=31.9\%$ , plastic limit  $w_P=18.8\%$  and plasticity index  $I_p=13.1$ . The moisture content is 18.83%. The saturated permeability of the sand-gravel is  $1.16 \times 10^{-4}$ . In addition, the grain size distribution curve is shown in Figure 2.

The large-size direct shear (LSDS) tests and triaxial tests of undisturbed soil specimens from the Beichuan slope were conducted in the soil laboratory following the procedures as described in BS1377:1990. For the soil in the surface slope, it contains large size of practices so that it is necessary to perform LSDS test. The superficial soil with engineering type of yellow is very dry, stiff and low cohesion and contains sandy gravel (maximum diameter = 50mm). The LSDS test was performed at a constant rate of 0.5mm/min until to a total horizontal displacement of 60mm. Four LSDS tests were carried out under normal pressures 25kPa, 50kPa, 100kPa, and 300kPa, respectively. Results of LSDS tests are presented in Figure 3. It can be observed from the results that the peak stress increases with increasing the normal stress; specifically under normal stress 300kPa, the maximum shear stress is 272.81kPa. Meanwhile a “stress-softening” can be clearly observed. In addition, totally twelve triaxial tests on four soils were carried out with constant strain rate. The sample was trimmed to 50mm in diameter and 100mm in height. Effective confining pressure (50kPa, 100kPa and 300kPa, respectively) was applied to consolidate the soil. The compression rate of 0.03mm/min was used to shear the specimens. Results of CU triaxial tests are presented in Figure 4 and the effective  $c, \phi$  values are determined in Table 2.

Table 1 Description of soils from Beichuan for triaxial tests

ID.	Depth (m)	Description
1-1	0~1.5	Fractured, yellow brown, sandy GRAVEL (max. dia. = 40 mm), no cohesion and very low wetness
1-2	1.5~6.5	Stiff, black brown, sandy CLAY, medium cohesion and wetness
1-3	6.5~12.9	Firm, yellow brown, very sandy GRAVEL (max. dia. = 20mm), with cohesion and very low wetness
1-4	12.9~19	Stiff, brown, sandy GRAVEL (max. dia. = 20 mm), no cohesion and very low wetness

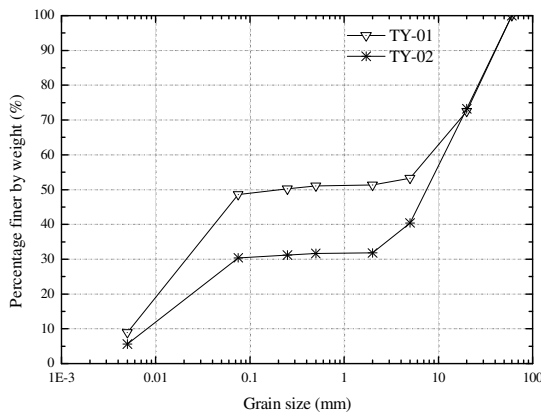


Figure 2 Grain size distribution curve

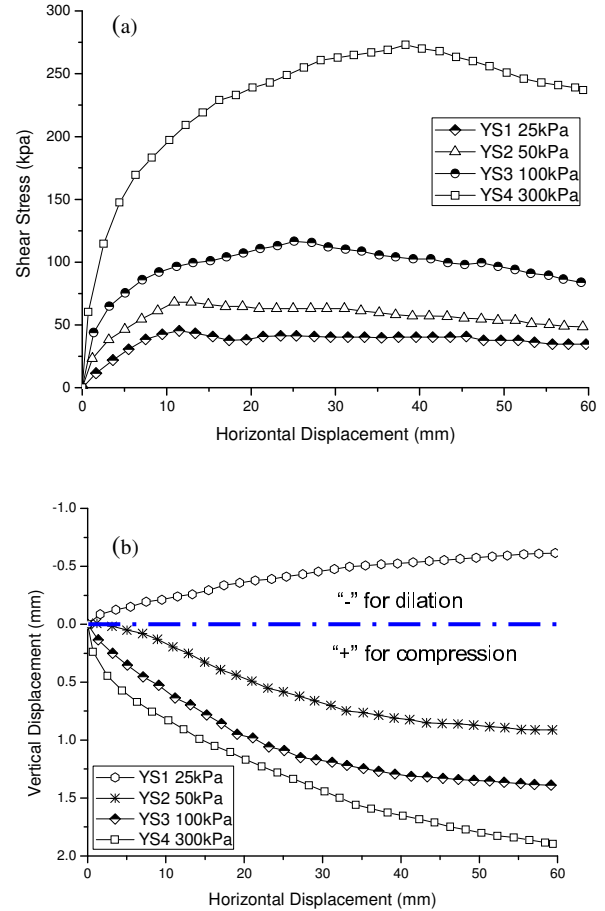


Figure 3 LSDS results for the yellow soil (a) horizontal displacement versus shear stress; (b) horizontal displacement versus vertical displacement

Relationships between axial strain and deviator stress are presented in Figure 4(a). It can be observed that the confining pressure has important impact on the stress-strain behavior. When the strain exceeds 10%, no obvious peak of shear strength appears for the specimens, while strain-softening can be observed for specimen 1-1. This maybe indicates that the soil specimen of 1-1 is little over-consolidated, whereas other soils are normally-consolidated with strain hardening property. Figure 4(b) presents the relationship between axial strain and excess pore water pressure (EPP). The gravel in soil makes the curves not quite consistent. The EPP of sample 1-4 under 200kPa effective confining pressure shows a slow increase at the beginning, and then an obvious sharp increase which might be because the high gravel contents in sample 1-4. When the gravel is under shear, low permeability makes the excess pore water hard to dissipate, thus increase the excess pore water pressure.

Relationships of mean effective stress and deviator stress are demonstrated in Figure 4(c). It can be seen that high deviator stress is obtained under high confining pressure, or rather the higher the mean effective stress, the higher the deviator stress. For all the curves, the effective stress paths bend to the right after failure, which indicates shear dilation. Shear dilation happens indicates the soils are undisturbed and their structures were well kept.

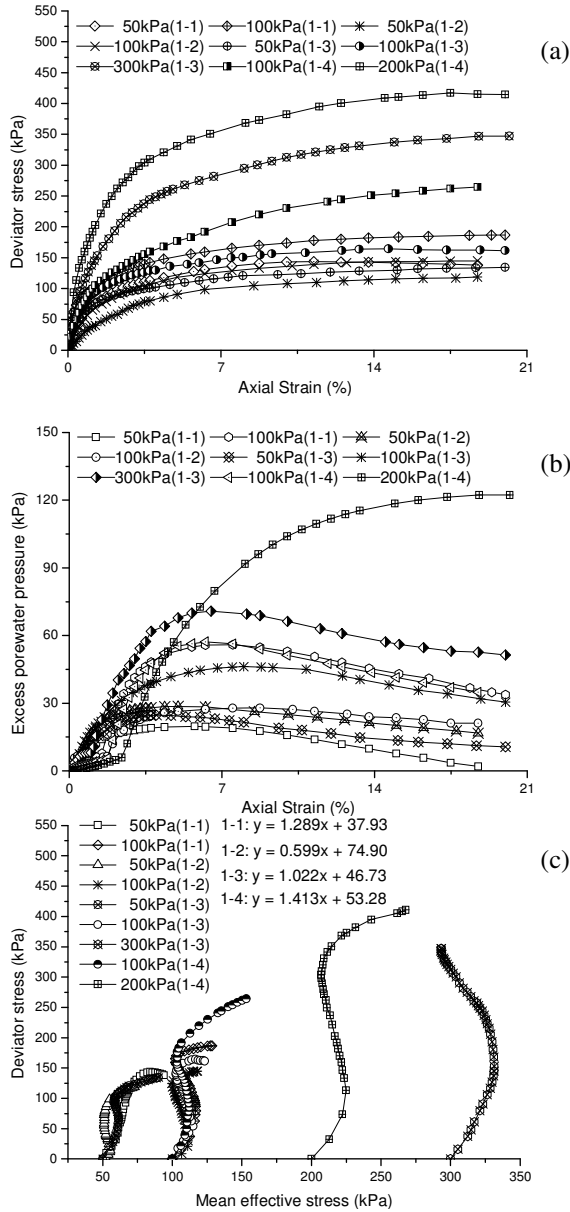


Figure 4 CU test results for Beichuan soils (a) axial strain versus deviator stress (b) axial strain versus excess pore water pressure (c) mean effective stress versus deviator stress

Table 2 Determination of  $c$ ,  $\phi$  values in triaxial tests

Sample ID	Line fitting	$c$ (kPa)	$\phi$ (deg)
1-1	$y = 1.289x + 37.93$	17.7	28.0
1-2	$y = 0.599x + 74.90$	35.3	15.2
1-3	$y = 1.022x + 46.73$	21.8	23.6
1-4	$y = 1.413x + 53.28$	24.8	29.8

## 4. DEVELOPING OF IN-PLACE INCLINOMETER WITH FBG SENSING TECHNOLOGY

### 4.1 Principle of the FBG sensor

The development of fiber optic sensing technology has drawn many attentions in civil engineering due to its advantages mentioned before. The fiber is made of fused silica and protected by the cladding (i.e. typically 125 $\mu$ m diameter) and coating. The inside

core is used for light travels with surrounding by the cladding. In this study, the sensing technology is based on the FBG sensors which are manufactured by phase mask method in the Hong Kong Polytechnic University. The fabrication details can be found in Zhu et al (2010a). The working principle of the FBG sensor is depicted in figure 5. As shown in the figure, when the ultraviolet light pass through the FBG sensor, a special narrow broadband light will reflect. The reflected wavelength is defined by

$$\lambda_B = 2n_{eff}\Lambda \quad (1)$$

where  $n_{eff}$  and  $\Lambda$  are the core index of refraction and the grating period of index modulation, respectively. The parameter  $n_{eff}$  and  $\Lambda$  will be changed with externally perturbations (i.e. strain and temperature), which will result in shift of wavelength. The wavelength shift  $\Delta\lambda_B$  is given by:

$$\begin{aligned} \frac{\Delta\lambda_B}{\lambda_B} &= [1 - p_e] \Delta\varepsilon + (\alpha + \xi) \Delta T \\ &= c_e \Delta\varepsilon + c_T \Delta T \end{aligned} \quad (2)$$

where  $p_e$  is the elastic optical coefficient;  $\alpha$  and  $\xi$  are the coefficients of temperature effect;  $\Delta\varepsilon$  and  $\Delta T$  are changes of strain and temperature;  $\lambda_B$  is the initial Bragg wavelength which is typically between 1510 nm and 1590 nm;  $\Delta\lambda$  is the variation of Bragg wavelength due to the applied strain and temperature;  $c_e$  and  $c_T$  are the calibration coefficients of strain and temperature which are obtained from the calibration tests. In this study, the calibration coefficients of  $c_e$  and  $c_T$  are  $0.78 \times 10^{-6} \mu\epsilon^{-1}$  and  $6.67 \times 10^{-6} \text{C}^{-1}$ , respectively.

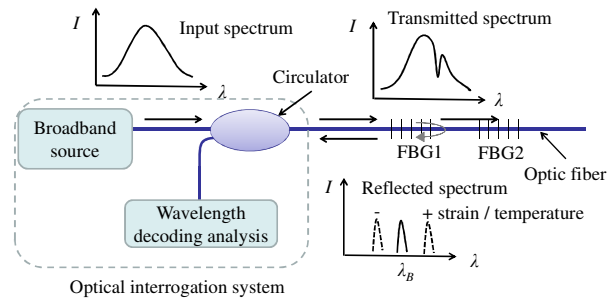


Figure 5 Working principles of FBG sensors

### 4.2 Principle of the in-place inclinometer with the FBG sensing bar

A resin bar (with diameter of 20mm and 1m length) was employed as the sensing bar. On the surface of the bar, two 'v-groove' were fabricated so that the FBG sensors can be glued and adhered on the sensing bar. Based on the strain results of the FBG sensors, the deflection and rotation at the free end can be calculated given the presences that the other end of the sensing bar was fixed. The calculation can be expressed as (Pei et al., 2012):

$$d_i = a\varepsilon_{i1} \quad (3)$$

$$\theta_i = b\varepsilon_{i2} \quad (4)$$

where  $d_i$  is the deflection of the  $i$ th smart bar;  $\theta_i$  is the rotation of the  $i$ th smart bar;  $a$  and  $b$  are two coefficients;  $\varepsilon_1$  and  $\varepsilon_2$  are the strains measured by the two different FBG sensors. A series of sensing bars will be connected with the steel tubes. The steel tubes are the same as traditional inclinometer probes which have two sets of wheels. The guided wheels will guide and orient the tube and FBG sensing bars along the PVC casing (Dunnicliff, 1998). With this connection method, the deflection at the upper connected point of the FBG sensing bar can be derived as follow:

$$d_i = d_{i-1} + L_{i-1} \tan \theta_i + (L_{i-1} + l_{i-1}) \tan \left( \sum_{i=1}^i \theta_i \right) \quad (5)$$

where  $d_i$  and  $d_{i-1}$  are the deflection of the  $i$ th and  $(i-1)$ th smart bar respectively;  $L_i$  and  $L_{i-1}$  are the length of the  $i$ th and  $(i-1)$ th steel bar respectively;  $l_{i-1}$  is the length of the  $(i-1)$ th smart sensing bar.

### 5. FIELD MONITORING RESULTS AND DISCUSSIONS

#### 5.1 Monitoring results of the FBG based in-place inclinometer

Two boreholes in this slope were equipped with FBG based in-place inclinometers. The schematic diagram of the monitoring system is shown in figure 6. For each borehole, six sets of the FBG sensing bars along with seven sets of steel tubes were connected in series and installed in both borehole A and B on 20 June 2010. As depicted in the figure 6, the FBG sensors of different depths in the one side of the sensing bar were connected through one fiber optic cable. Totally, two fiber optic cables were used to connect all the FBG sensors in each borehole A and B. Then, four cables connected with the interrogator through around 1 km armored cables. The interrogator was placed in a monitoring station (around 1 km from the slope). All the monitoring works were conducted in the station room. The initial wavelengths of all FBG sensors were taken on 20 June 2010 and the flowing readings were taken sequentially.

According to the equation (2), the strains of the FBG sensors were calculated based on the wavelengths results and then the deflections of the sensing bar can be obtained through equation (5) by iterative method. The cumulative displacement results of both borehole A and B from 14 July to 25 September are shown in figure 7. As observed in the figure, the cumulative displacements increase with the depth in both boreholes A and B except that the surface point of the borehole were reinforced by the concrete box. In the figure 7(b), the cumulative displacement at the attitude 939m is smaller than displacement at attitude 937. The behind reason of this phenomenon might be attributed to the geology condition. According to the site investigation, the dynamic penetration tests results are shown that the penetration resistance at elevation of 939m is much larger than that at 937m. The displacement results of borehole A are much larger than that of borehole B. This phenomenon can be mainly attributed to progressive failure of loose geo-materials. After the earthquake and heavy rainfall, the shear strength of the soil in the slope decreased dramatically. Furthermore, the heavy rainfall will increase the water table and yield or increase positive water pressure. The rainfall infiltration will reduce the matric suction in soil which in turn reduces the shear strength of soil (Li et al., 2005; Lee et al., 2009). All these factors will induce the failure of the slope. Since the deflections were significant related to the rainfall, it is necessary to investigate the relationship between the rainfall and the displacement in the following study.

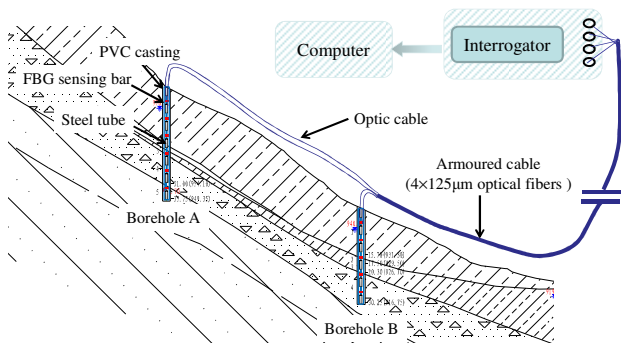


Figure 6 Diagram of monitoring system

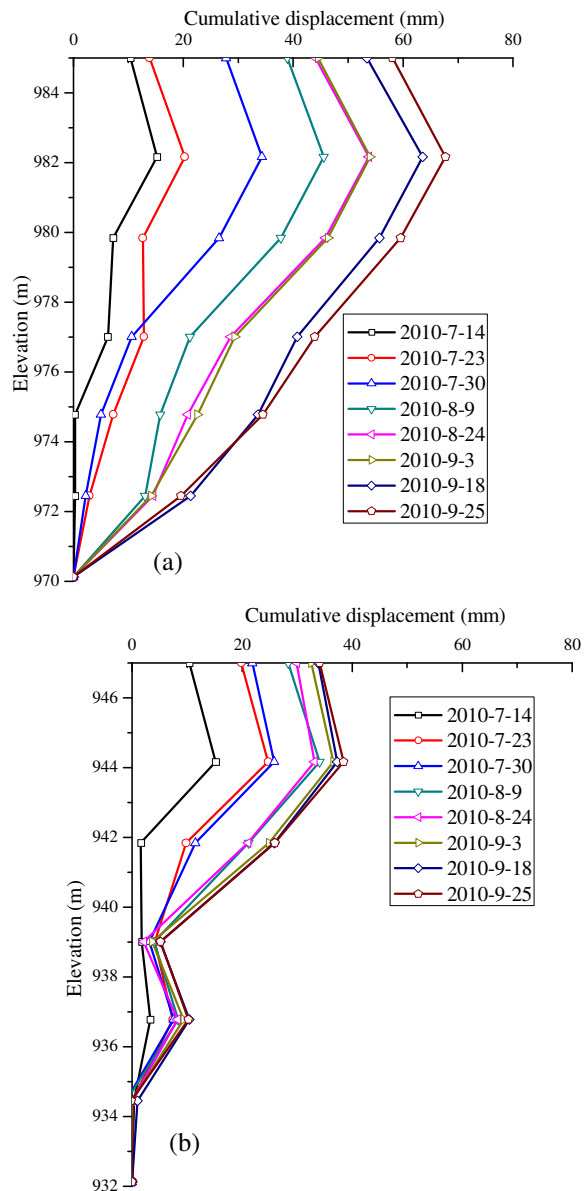


Figure 7 Results of in-place inclinometers: (a) Deflections of Borehole A; (b) Deflections of Borehole B

#### 5.2 Displacement analysis with rainfall data

An automatic rainfall gauge was installed close to the monitoring station. The rainfall data was collected during monitoring period (from 27 June to 24 September 2010) in this slope. To investigate the rainfall effect on the slope stability, the cumulative displacements versus time along with daily rainfall are shown in the figure 8. As observed from the figure, the displacements have an apparent relationship with the daily rainfall as the displacements increase with the daily rainfall for both boreholes A and B, especially in the period from July 26 to August 22. By comparing the results at different depths, it can be found that the effect of rainfall has higher impact on the surface slope (i.e. above 5.16m). This is probably because the shallow failures can be generated by the short rainfall while deep-seated geo-material has less been affected by the rainfall. The movement of deep-seated geo-material is normally induced by the long-term variation of annual rainfall (Pietro, 2004).

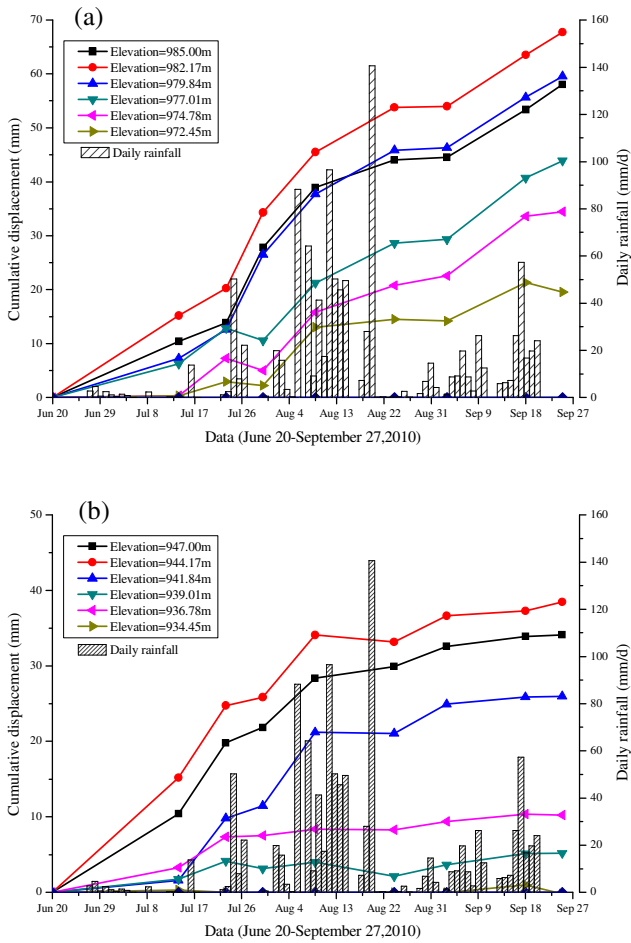


Figure 8 Relationship between displacement distribution and rainfall: (a) Displacement at different depths and the rainfall of Borehole A; (b) Displacement at different depths and the rainfall of Borehole B

**6. IEFFECT OF RAINFALL INTENSITY AND DURATION ON THE STABILITY OF SLOPE**

Based on the geology investigation and mechanical properties of geo-materials conducted before, the finite element model was established to analyze effect of rainfall intensity and duration on the stability of slope. The commercially software SEEP/W and SLOPE/W (GeoSlope International Ltd., 2004) were used to perform seepage analysis and stability analysis, respectively. The slope geometry and boundary conditions are shown in figure 9. The initial water table was defined based on the information of borehole A and B, which are both 6.6m below the top of borehole. As depicted in the figure 9, the boundary condition of unit flux  $q$  was applied on CD (i.e. surface of the slope) to simulate rainfall intensity, no flow zone boundary conditions were applied on sides of slope above water table and bottom of the slope; meanwhile, the total head boundary was used for the boundary sides of slope below the water table. In addition, the volumetric water contents various with suction between zero and -100kPa can be estimated by the Fredlund and Xing equation (Fredlund and Xing, 1994).

$$w(\psi) = C(\psi) \frac{w_s}{\{\ln[e + (\psi/a)^n]\}^m} \quad (6)$$

where  $w(\psi)$  is the water content at any soil suction;  $w_s$  is the saturated water content; and  $a$ ,  $n$ , and  $m$  are fitting soil parameters associated with the soil-water characteristic curve (SWCC). The variable  $e$  is the base of the natural logarithm. The correction factor,  $C(\psi)$ , is written as follows:

$$C(\psi) = 1 - \frac{\ln(1 + \psi / \psi_r)}{\ln(1 + 1000000 / \psi_r)} \quad (7)$$

where  $\psi$  is any soil suction value and  $\psi_r$  is soil suction at residual conditions. Both have a unit of kPa.

The closed-form solution of this equation will be employed to derive the volumetric water content function based on the three parameters  $a$ ,  $n$  and  $m$ . In this study, the saturated hydraulic conductivity  $k_s$  was equal to  $10^{-4}$  m/s and  $a=5$  kPa,  $m=1$ ,  $n=1$ . The unsaturated hydraulic conductivity function was predicted by the Fredlund et al. (1994). In addition to the hydraulic parameters, the shear strengths parameters of the soils were determined by the previous laboratory tests.

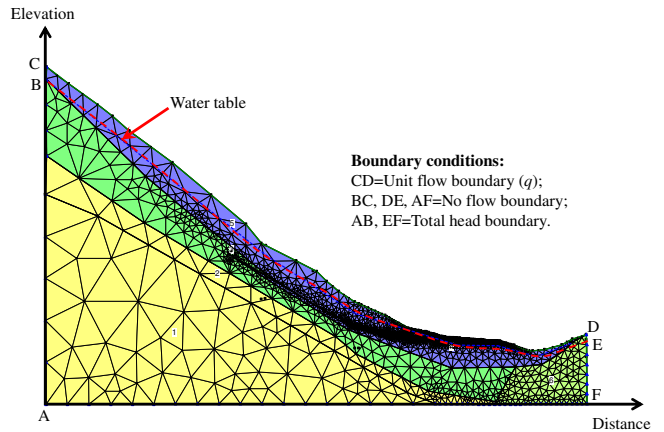


Figure 9 Geometry and boundary conditions of the slope

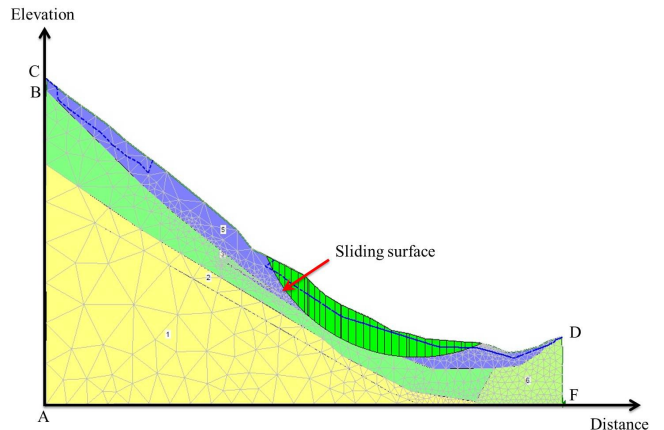


Figure 10 Sliding surface in the slope stability analysis

The factor of safety ( $FOS$ ) of the slope was examined under different rainfall intensity and duration based on the same parameters of  $a$ ,  $m$ ,  $n$  and  $k_s$ , but the unit flux are different according to the various rainfall intensity. The sliding surface in the slope stability analysis was shown in figure 10. In order to reduce the effect of geometry and uniform boundary conditions on the analysis results, the normalized factor of safety  $F_{sn}$ , which is the factor of safety at each time step divides by the initial value of  $FOS$ , was used in comparing and analyzing in the different unit flux conditions. The  $F_{sn}$  versus rainfall duration at different intensities were shown in figure 11. As observed in the figure, the rainfall intensity has a strong effect on the slope stability. When the rainfall intensity higher (or equal) than 0.5mm/h, the  $F_{sn}$  decrease with the increasing of rainfall duration. It is worth noting that the  $F_{sn}$  dramatic decreased at rainfall duration longer than 100h for the rainfall intensity ( $I_r$ ) at 0.1 and 1.0mm/h. It can be observed that the rainfall infiltration has an essential impact on slope stability when the daily rainfall exceeds 20mm/d.

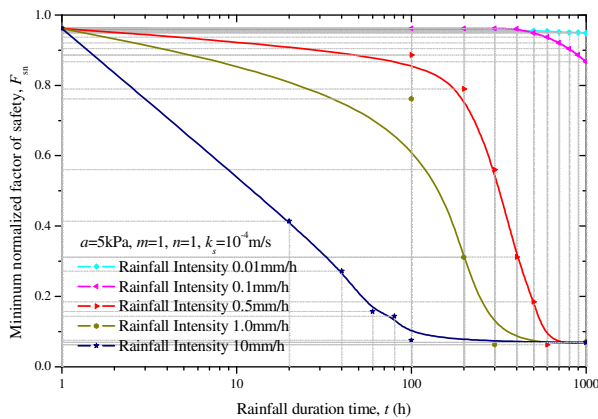


Figure 11  $F_{sn}$  under different rainfall duration

## 7. CONCLUSIONS

After the earthquakes and heavy rainfall had struck the Beichuan area, a disaster of debris flow happened in the Weijia gully. Geotechnical investigations were carried out after the debris flow. Two boreholes were drilled and soil samples were taken for a series of laboratory tests. Additionally, a new inclinometer based on the FBG sensors have been developed and applied for long-term displacement monitoring of a slope in the Weijia gully. The displacements of the slope along with the rainfall data were recorded and analyzed. The main findings through this study are presented below.

- The monitoring results of FBG based in-place inclinometers indicate that the rainfall infiltration has a close relationship with the internal displacements of the slope. The cumulative displacements of both boreholes were increased quickly in the rainy season (i.e. from July to August, 2010).
- The rainfall infiltration had an important impact the surface slope, but the influence decreased dramatically when the depths exceed 5.2m for both borehole A and B.
- The results of LSDS and triaxial tests of soil specimens taken at different depths of the slope site provide soil parameters for finite element analysis of the slope.
- The finite element simulation demonstrates that slope stability decreases significantly when the rainfall intensity is higher (or equal) than 0.5mm/h and rainfall duration is longer than 100h. It shall be paid attention to the slope movement when the rainfall intensity exceeds the saturated permeability  $k_s$ .

## 8. ACKNOWLEDGEMENT

Financial supports (85G0, G-U960, G-YJ99, 1-BB7U) by The Hong Kong Polytechnic University and the Chinese National Science Foundation (Grant No. 10972166) are acknowledged.

## 9. REFERENCES

BS 1377. (1990). "British Standard BS1377: Methods of test for soils for civil engineering purposes." *British Standards Institution* (BSI), London, UK.

BS 1377-2. (1990). "Methods of Test for Soils for Civil Engineering Purpose-Part 2: Classification Tests." *British Standards Institution* (BSI), London, UK.

Chang, M. (2002). "A 3D slope stability analysis method assuming parallel lines of intersection and differential straining of block contacts." *Canadian Geotechnical Journal*, 39, pp799-811.

Collins, B. D. and Dobroslav, Z. (2004). "Stability analysis of rainfall induced landslides." *J. of Geotech. and Geoenvironment. Eng.*, 130(4), pp362-372.

Cui P, Chen X. Q, Zhu Y.Y, Su F.H., Han Y.S., Liu H.J., Zhuang J.Q. (2011). "The Wenchuan Earthquake (May 12, 2008), Sichuan

Province, China, and resulting geohazards." *Natural Hazards*. 56:19-36.

Dunncliff J. (1993). "Geotechnical Instrumentation for Monitoring Field Performance." New York: Wiley-Interscience, pp 252

Frattoni, P., Crosta, G. and Sosio, R. (2009). "Approaches for defining thresholds and return periods for rainfall-triggered shallow landslides." *Hydrological Processes*, 23(10), pp1444-1460.

Fredlund, D.G., and Xing, A. (1994). "Equations for the soil-water characteristic curve." *Canadian Geotechnical Journal*, 31(4), pp521-532.

Fredlund D.G., Xing A., and Huang S. (1994), "Predicting the permeability function for unsaturated soils using the soil-water characteristic curve." *Canadian Geotechnical Journal*, 31(3):pp521-523

GeoSlope International Ltd., (2004). "Seep/W User's guide for finite element seepage analysis." *GEO-SLOPE international Ltd.*, Calgary, Alta.

Greco V. R. (1996). "Efficient Monte Carlo technique for locating critical slip surface." *J. Geotech. Eng. ASCE*, 122(7), pp517-25.

Hill, K.O., Fujii, Y., Johnson, D.C. and Kawasaki, B.S. (1978). "Photosensitivity in optical fiber waveguides: application to reflection filter fabrication." *Applied Physics Letters*, 32(10), pp647-649.

Hovland, H.J. (1977). "Three-dimensional slope stability analysis method." *Journal of Geotechnical Engineering Division*, Proceedings of the American Society of Civil Engineers, 103, pp971-986.

Huang, C. C., Tsai, C. C. (2000). "New method for 3D and asymmetrical slope stability analysis." *Journal of the Geotechnical and Geoenvironmental Engineering*, ASCE, 126(10), pp917-927.

Lee Min Lee, Nurly Gofar, harianto Rahardjo. (2009). "A simply model for preliminary evaluation of rainfall-induced slope stability." *Engineering Geology*, 108, pp272-285.

Leonardo Cascini, Michele Calvello, and Giuseppe M. Grimaldi. (2010). "Groundwater Modeling for the Analysis of Active Slow-Moving Landslides." *J. Geotech. and Geoenviron. Eng.* 136, pp1220-1230.

Li, A. G., Tham, L.G, Yue, G.Q. Lee, et al. (2005). "Comparison of field and laboratory soil-water characteristic curves." *Journal of geotechnical and Geoenvironmental Engineering*, ASCE, 131(9), pp1176-1180.

Morgenstern NR, Price VE. (1965). "The analysis of the stability of general slip surfaces." *Geotechnique*, 15(3), pp79-93.

Pei H.F., Yin, J.H., Zhu, H.H., Hong, C.Y., Jin, W., and Xu, D.S. (2012). "Monitoring of lateral displacements of a slope using a series of special fibre Bragg grating-based in-place inclinometers." *Measurement Science and Technology*, 23 doi:10.1088/0957-0233/23/2/025007

Pietro Aleotti. (2004). "A warning system for rainfall-induced shallow failures." *Engineering Geology*, 73, pp247-265.

Rahardjo, and Eng-Choon Leong. (2010). "Effect of hydraulic properties of soil on rainfall-induced slope failure." *Engineering Geology*, 114, pp135-143.

Sarma S. K. (1973). "Stability analysis of embankments and slopes." *Geotechnique*, 23, pp 423-33.

Tohari, A., Nishigaki, M. and Komatsu, M. (2007). "Laboratory rainfall induced slope failure with moisture content measurement." *J. of Geotech. and Geoenvironment. Eng.*, 133(5), pp575-587.

Yin Y.P. (2008). "Research on the geo-hazards triggered by Wenchuan earthquake, Sichuan." *Journal of Engineering Geology*, 16 (4)-0433-12.

Yin J H, Zhu H H, Fung K. W, Jin W, Mak L M, and Kuo K. (2008). "Innovative optical fiber sensors for monitoring displacement of geotechnical structures." *The HKIE Geotechnical Division 28th Annual Seminar*, Hong Kong, pp287-294

Zhang, X. (1988). "Three-dimensional stability analysis of concave

- slopes in plan view.” *Journal of Geotechnical Engineering*, 114, pp658-671.
- Zheng H., Sun G, and Liu D. (2009). “A practical procedure for searching critical slip surfaces of slopes based on the strength reduction technique.” *Comput Geotech*, 36, pp1-5.
- Zhu H H, Yin J H, Zhang L, Jin W, and Dong J H. (2010a). “Monitoring internal displacements of a model dam using FBG sensing bars.” *Adv. Struc. Eng.* 13(2), pp249-261
- Zhuang J.Q., Cui P., Hu K.H., Chen X.Q., Ge Y.G. (2010) “Characteristics of Earthquake-Triggered Landslides and Post-Earthquake Debris Flows in Beichuan county.” *Journal of Mountain Science*, 7(3):pp246-254.